Rare Met. (2025) 44(4):2845–2852
https://doi.org/10.1007/s12598-024-03128-3

RARE METALS

LETTER

Observation of dislocation-mediated plastic deformation in TiMoN coating

Sheng-Hao Zhou, Zhao-Guo Qiu, Zhen-Yu Wang*, Wei Yang, Ai-Ying Wang*

Received: 30 August 2024 / Revised: 23 October 2024 / Accepted: 30 October 2024 / Published online: 21 February 2025
© Youke Publishing Co., Ltd. 2025

The recently established theory has built clear connections between hardness and toughness and electron structure involving both valence electron concentration (VEC) and core electron count (CEC) in transition metal nitride (TMN) ceramics. However, the underlying deformation mechanisms remain unclear. Herein, we conduct in-depth analysis on microstructure evolution during deformation of the high VEC–CEC solution TiMoN coatings having desired combination of high hardness and toughness. The effects of solid solution, preferred orientation linked with symbiotic compressive stress, grain size and dislocations are systematically discussed. We discover that numerous dislocations have been implanted into the nanocrystals of the TiMoN coating during the high-ionization arc deposition. Using two-beam bright-field imaging, we count the dislocation density and confirm occurrence of dislocation multiplication to form effective plastic deformation, which contributes to significant strain hardening, comparable to solid solution hardening, fine-grain hardening and compressive stress hardening. The improved dislocation activities also play a crucial role in enhancing the toughness by providing extra energy dissipation paths. This work gains new insights into the origins of mechanical properties of ceramic coatings and possibility to tune them via defects.

Owning high hardness, excellent wear resistance and strong oxidation resistance, transitional metallic nitride (TMN) hard coatings have been extensively employed to prolong the durability of key components used in extremely harsh conditions, such as cutting tools, drills and engine blades etc. With poor coordinated deformation ability, however, TMN coatings suffer from low toughness, which can even embrittle the coated substrates [1]. Therefore, it is a perennial and important issue to promote the toughness and thus to obtain a promoted load-bearing capacity of TMN coatings.

To date, many attempts have been elaborated to improve the toughness of TMN coatings [2–5]. Among them, solid solution with heavy early-transitional metal (ETM) including W [6–8], Mo [9–11], Ta [12] and Nb [13] has shown advantage to break through the hardness-toughness paradox. Recently, a guiding theory for solid solution design of TMN has been established, showing reliable connection attributing the simultaneous enhancement of hardness and toughness to the enhanced occupation of both covalent and metallic orbits, which is caused by the high valence electron concentration (VEC) and core electron count (CEC) of the solution elements. This theoretical prediction has been attested by numerous experimental results before and after [8, 9, 13–17].

Supplementary Information The online version contains supplementary material available at https://doi.org/10.1007/s12598-024-03128-3.

S.-H. Zhou, Z.-Y. Wang*, W. Yang, A.-Y. Wang*
Key Laboratory of Advanced Marine Materials, Ningbo Institute of Materials Technology and Engineering, Chinese Academy of Sciences, Ningbo 315201, China
e-mail: wangzy@nimte.ac.cn

A.-Y. Wang
e-mail: aywang@nimte.ac.cn

S.-H. Zhou
e-mail: tomhmot@163.com

S.-H. Zhou, Z.-G. Qiu
School of Materials Science and Engineering, South China University of Technology, Guangzhou 510640, China

Z.-Y. Wang, A.-Y. Wang
Center of Materials Science and Optoelectronics Engineering, University of Chinese Academy of Sciences, Beijing 100049, China

Whereas, the actual mechanical properties of TMN coatings often deviate from theoretical prediction, because other factors, like plastic deformation-related processes, also have significant influences. There still lack fundamental understanding on such correlations till now. It might be due to that many TMNs behave in highly elastic manners. For physical vapor deposition (PVD)-deposited TMN coatings owning typical nanocrystalline columnar structure, the deformation has been observed to be dominated by grain boundary (GB) activities, such as GB sliding and rotation [18, 19] as well as intergranular cracking [20], without obvious intragranular plasticity. A recent work by Chen et al. [21, 22] shows that high density of dislocations can be created inside the brittle superlatticed TiN/AlN single crystal, although no apparent differences can be seen between its deformation with those of previously reported TMN coatings [20] from morphological sight.

In this work, we focus on the investigation of deformation mechanisms of the model material-$TiMo_{27}N$ coating, which possesses a desired combination of high hardness and toughness due to high fraction solution of the high VEC–CEC Mo element. By performing systematic indentation tests and in-depth transmission electron microscope (TEM) characterization, we identify the activation of dislocation-mediated plasticity during indentation deformation and its significant roles on both hardness and toughness. Mechanical mechanisms with respect to solid solution, grain size, orientation and compressive stress are also discussed in details.

The $TiMo_{27}N$ coatings were deposited by a home-made multi-arc ion plating system supplied with alloyed $Ti_{73}Mo_{27}$ targets at a N_2 working pressure of 1.6 Pa. Mirror-polished cemented carbide (WC: 90 wt%, Co: 10 wt%) cubes were used as substrates. Prior to deposition, all substrates were ultra-sonically cleaned in ethanol liquid for 20 min to remove adhesive contaminants. The base pressure of chamber was about 7×10^{-3} Pa, and temperature was maintained at 250 °C. After that, an Ar^+ etching process was conducted at a direct-current (DC) pulsed bias of −500 V to improve coating adhesion strength. The actual composition of the as-deposited coating is $Ti_{31.5}Mo_{9.1}N_{59.4}$ determined by energy-dispersive spectroscopy (EDS), indicating a fraction of Mo loss during deposition. Phase structure of the coating was examined by a grazing incident X-ray diffraction (GIXRD) method in Rigaku Smartlab with a Cu-K_α source. Transition electron microscope (TEM, FEI TALOS-200 kV) was employed to investigate the pristine and deformed microstructure of $TiMo_{27}N$ coatings. Dislocations were observed using two-beam bright-field (BF) imaging technique. The TEM foil samples were prepared by focused ion beam (FIB) lifted-up technique.

Mechanical properties were acquired by nanoindentation tests (CSM, Anton Paar) using Berkovic indenter with a constant load mode at 5 mN. All indentation depths were less than 150 nm, below one tenth of coating thickness, to minimize the influences from the substrates. Vickers indentation tests were carried out to evaluate the crack resistance of coatings. A high load of 200 gf was used. Additionally, sharp cube-corner indenter was also performed to probe toughness and induce severer plastic deformation in a smaller volume. An extremely high load of 400 mN was used for approaching the cracking limit of the coating, where the surface profiles were visualized by atom force microscope (AFM).

Figure 1 shows the XRD pattern of the as-deposited $TiMo_{27}N$ coating, indicating that the $TiMo_{27}N$ coating has a dual-phase structure comprising the predominating B1 face-centered cubic (fcc)-TiN phase and a small amount of body-centered tetragonal (bct)-Ti_2N phase. This is different from the previous theoretical results that assumed a single fcc phase structure of TiMoN system [9, 15]. The fcc phase shows strong (111) preferred orientation, which is a typically seen strain energy-predominant feature. Its formation is associated with the strong ion bombardment effect generated during the arc ion plating process, which facilitated structural densification and growth of compressive stress due to massive adatom inserting into and pinning the grain boundaries (GBs) [23]. The resulting compressive stress of the current $TiMo_{27}N$ coating reached 3 GPa, determined by substrate curvature method using Stoney equation [24]. In fcc-TiN crystalline, the (111) plane possessed the lowest strain energy but highest surface energy [25]. When stressed in compressive state, the columnar grains tend to evolve along preferential (111) planes to reduce the strain energy of GBs. It was noticeable that although the fraction of bct-Ti_2N phases was quite small, it could deteriorate the toughness of coating because of the large lattice misfits at bct-fcc interfaces [26].

As clearly presented in the bright-field (BF) image in Fig. 1b, the $TiMo_{27}N$ coating has a dense, nanocrystalline columnar structure. The inserted selected-area electron diffraction (SAED) shows the sole existence of fcc main phase, with Ti_2N phase absent. It might be because that the Ti_2N phase is in extremely fine-needle shape dispersed among the fcc matrix (further details are referred to Ref. [26]). The grain size was determined by counting the width of about fifty grains from the BF images, yielding an average grain size of 56.5 ± 25 nm (Fig. 1c). The high-resolution TEM (HRTEM) images (Fig. 1d, e) further reveal dominating (111) orientation for most of columnar grains. All these SAED patterns, as depicted in Fig. 1d1, e2, presented the identical [110] crystallographic zone axis with (111) plane perpendicular to the growth direction, which agreed well with the XRD results. Since the (111) orientated GBs comprise most of interface areas, the overall surface energy is increased. Consequently, it

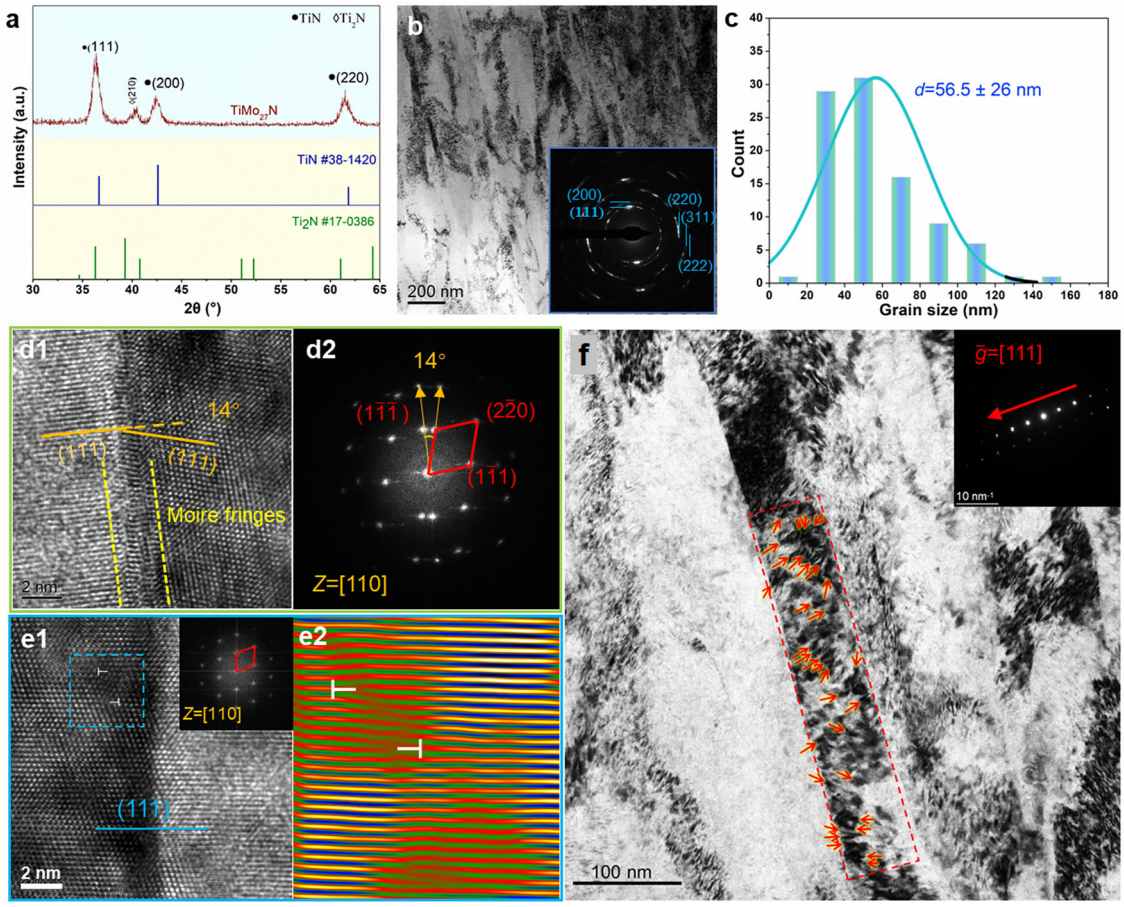

Fig. 1 **a** XRD pattern of the as-deposited $TiMo_{27}N$ coatings; **b** BF TEM morphology of $TiMo_{27}N$ coating; **c** grain size distribution; **d** evidence of LAGB by atomic HRTEM image and SAED patterns; **e1** rotation GB with in-plane coherent GB but out-of-plane misorientation; **e2** corresponding IFFT; **f** identifying multiple nanoscale dislocation conserved by high-energy deposition through two-beam BF imaging under $\boldsymbol{g}$ = [111]

facilitates a strong tendency to form lower-energy GB (LEGB) configurations. For example, Fig. 1d showcases a low-angle GB (LAGB), with the angle between two adjacent (111) planes being about 14.5°. The small angle forms a recognizable Moire fringes when the lattice overlaps at the GB. Figure 1e1 shows a second type of LEGB, (111) in-plane coherent rotation GBs. We can see that the lattice fringes of the left-side grain can extend across the GB to the right-side grain, but soon becomes blurry, as it is off-axis with the left-side grain at out-of-plane direction by a small angle. The HRTEM image and corresponding inverse-FFT image (Fig. 1e1, e2) capture a pair of misorientation dislocations near GB.

Two-beam BF imaging was conducted to figure out the intragranular dislocation structure. Surprisingly, we found numerous nanoscale dislocations inside the as-deposited nanograin (Fig. 1f). These dislocations or their resolved components all array along the long side of columnar grains with length over 100 nm, that offers enough space for storing dislocations. With $\boldsymbol{g}$ = [111] and the slipping plane parallel to (111), the Burgers Vector should be $\boldsymbol{B} = 1/2a[110]$. We have examined four more nanograins under two-beam BF condition (they are shown in Fig. S1) to see analogous structure. The dislocation density was then determined to be $(1.90 \pm 0.87) \times 10^{11}$ cm^{-2}, counted from a total area of 57,955 nm^2. These observations verify a previously overlooked fact that the fast nonequilibrium deposition plus ion bombardment implants plenty of crystal defects into the as-deposited coatings. Meanwhile, we suppose point defects should also ubiquitously exist [27], yet very hard to visualize. But our analysis didn't find any planar defects like stacking faults (SFs) or twins. Because the stacking fault energy (SFE) of ceramic is extremely high, formation of SFs or twins is exceptionally difficult and so the plentiful deposition-stored dislocations can't form extension either. We speculate that the strengthened metallic bonding due to high fraction of Mo solution also contributes to the dislocation storing ability of these nanograins.

Comprehensive mechanical behaviors were probed via indentation-based tests. The hardness and elastic modulus of the coating derived from nanoindentation tests is 33 ± 5

GPa and 483 ± 56 GPa, respectively. The hardness is approximately 10 GPa higher than hardness of pure TiN (23 ± 0.8 GPa). The Vickers indentation result (Fig. 2a) shows a nearly crack-free morphology under load of 200 g (1.98 N), except for an extremely narrow and short crack can be seen. Nanoindentation using cube corner provides a more accurate evaluation of crack resistance because the effect of substrate is minimized. As shown in Fig. 2b, the coating remains crack-free after indented under a high load of 400 mN. Instead, the large pile-up phenomena at indent edges can be seen, indicating strong plastic deformation ability.

To further understand the deformation mechanisms, we performed load-controlled nanoindentation under various strain rate ranging from 0.00417 to 0.0833 s^{-1}. Figure 2c shows the representative load–displacement curves. As shown in Fig. 2d, the strain rate sensitivity (SRS) index m is 0.009, indicating a rate-insensitive behavior. For typical metal like fcc-Cu [28], high m values are observed when grain size is refined to nanoscale due to enhanced resistance for dislocation and GB sliding [29, 30]. Conversely, brittle materials like ceramics and metallic glass often exhibit negative m values due to formation of large-sized shear band and cracks during deformation [31]. For nanograined nitride ceramic coatings, GB sliding [32] and intergranular cracking [33] have been frequently observed. Obviously, the small positive m implies effective suppression of intergranular cracking and possibly activation of plasticity.

To precisely understand deformation mechanisms, in-depth microstructural investigations have been performed. Figure 3 shows the cross-sectional TEM morphology of Vickers and cube-corner prints. As seen in Fig. 3a, the coating–substrate interface remains intact after deformation, showing strong adhesion strength of the coating. Shear steps formed at the bottom mark the occurrence of typical GB sliding. The curved columnar grains in the severely deformed area (Fig. 3b) indicate that the coating has strong plastic deformation ability. No phase transformation has been found. Meanwhile, GB rotation also occurred. Figure 3c exhibits a representative that the left-side grain totally off-axis with the right-side one. Figure 3d

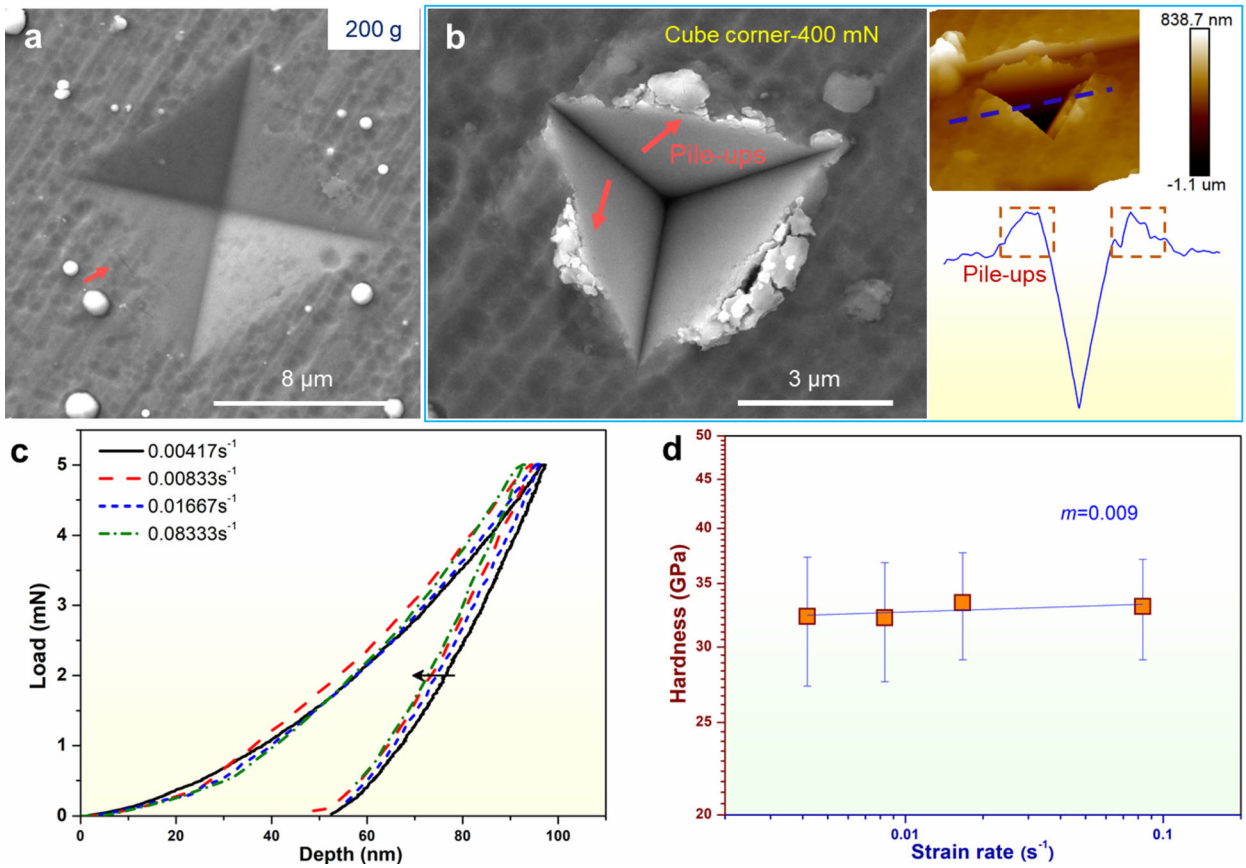

Fig. 2 **a** Vickers print under 200 g showing a nearly crack-free except for a narrow and small one pointed by red arrow. **b** Morphology of cube corner under 400 mN. Surface and line scan clearly show pile up at the edges. **c** Representative load–depth curves of TiMoN coatings taken from load control mode. The arrow indicates the rising strain rate. **d** log–log plotting of hardness as a function of strain rate. The slope represents strain rate sensitivity, m

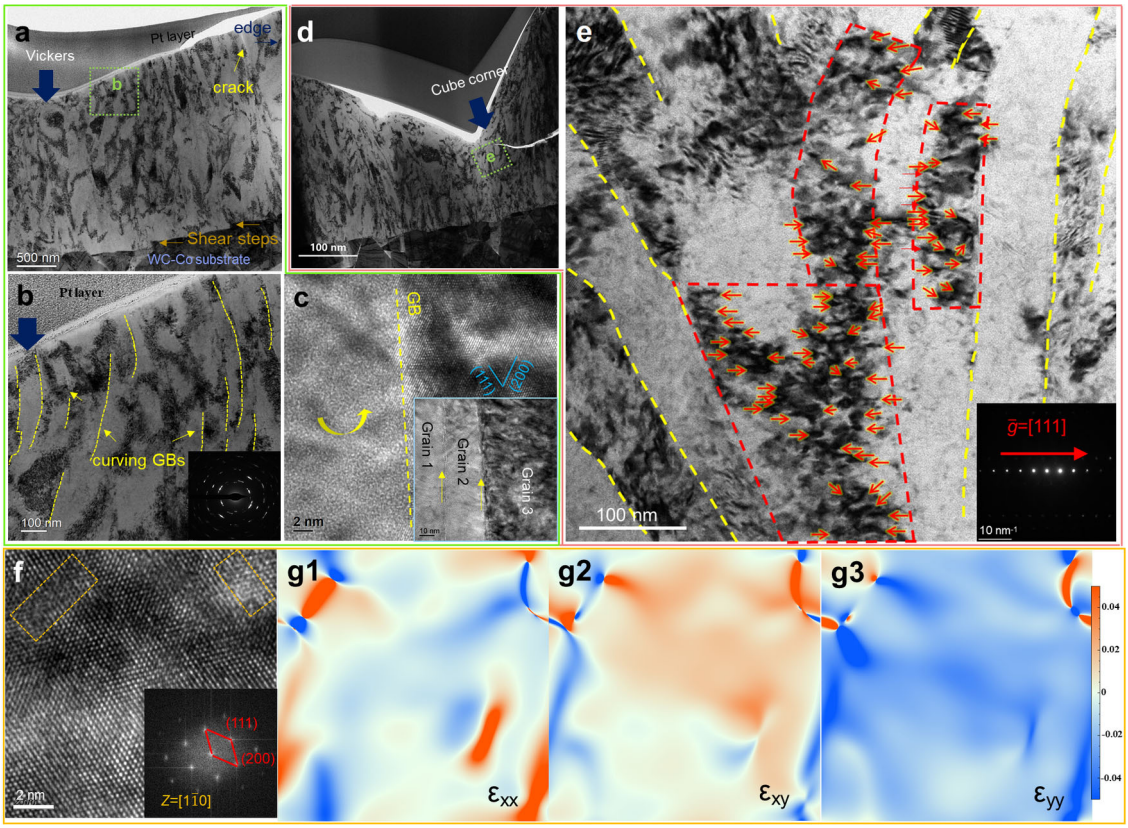

Fig. 3 **a** Cross-section TEM morphology of deformed structure under Vickers print, **b** enlarged image showing curved GBs. **c** HRTEM image showing rotated GB and the inserted image indicate its location. **d** Deformed structure under cube-corner print. **e** Enlarged image of curved GBs and high-density dislocation under two-beam condition ***g*** = [111]. **f** HRTEM image showing deformed area and **g** corresponding strain maps of horizontal (ε_{xx}) and vertical (ε_{yy}) normal strain, and shear strain (ε_{xy}), showing highly strained areas correspond to severe distortions in raw HRTEM image

demonstrates the cross section of cube-corner indentation print, for comparison. We can see that no intergranular cracks can be found in either the cube-corner indentation (Fig. 3d) or the Vickers indentation (Fig. 3a), testifying the deduction that cracking during deformation causing negative *m* of ceramics has been suppressed. On the other hand, the positive but low *m* value indicates possible dislocation mechanism aside the activating GB sliding.

Next, focus has been put on the severely deformed area right under the tip. Figure 3e exhibits the morphology enlarged from green-boxed area in Fig. 3d. The yellow dashed lines profile the analogous curved GBs, confirming occurrence of plastic deformation. More importantly, high-density nanoscale dislocations were observed inside the nanograins under two-beam BF with ***g*** = [111]. By counting the number of dislocations within a certain area (as marked by red dashed boxes in Fig. 3e), the average dislocation density was determined to be $(2.88 \pm 1.24) \times 10^{11}$ cm^{-2} after examining a total deformed area of 82,536 nm^2 (see Fig. S2 for more evidences), which yields a 50% increment after deformation (Fig. 4a). Note that no extended partials or stacking faults

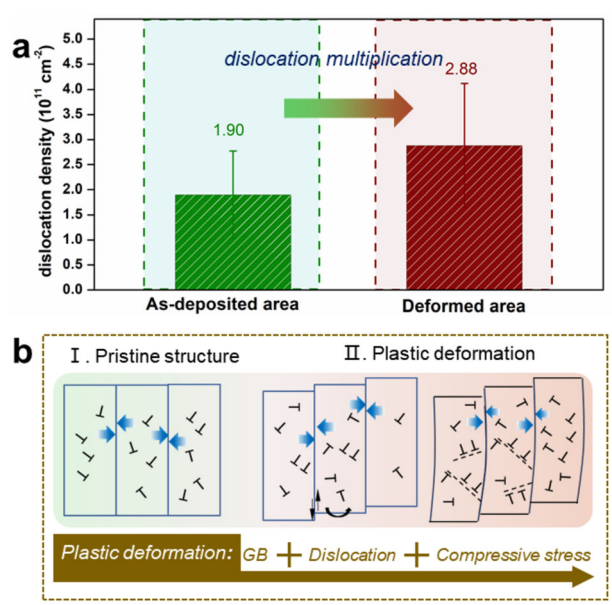

Fig. 4 **a** Statistical results of dislocation density before and after deformation in TiMoN coating. **b** Schematic illustration of deformation mechanisms of hard-yet-tough TiMoN system

have been found. We performed geometry phase analysis (GPA) to investigate the influences of dislocation cores on strain distribution in a deformed area with local distorted lattices (Fig. 3f). The resulting strain map in Fig. 3g1–g3 reveals that local strains appears at the same location of distorted areas where dislocations exist in Fig. 3f, while the rest areas remain less strained, in good agreement with the raw HRTEM image (Fig. 3f). Note that the scale of elastic strain field of TiMoN is quite small, accounting for the reason that TiMoN lattices are capable to contain large amounts of dislocations.

The above observations unambiguously verify the occurence of dislocation multiplication, along with concurrent GBs sliding in the nanocrystalline TiMoN coating, which has been sparsely discussed in previous studies. Dislocation multiplication increases the total slipping distances, and consequently offset the diffusion effect of GB sliding, ultimately leading to an extremely low m value. In addition, the observed dislocation activities have significantly influences on both hardness and toughness, which is discussed in the following.

On one hand, dislocation multiplication can cause strain hardening. Together with solution hardening, residual stress and GB hardening, the hardness of nanocrystalline $TiMo_{27}N$ coating can be expressed as $H = H_{theo} + \Delta\sigma_{stress} + \Delta\sigma_{HP} + \Delta\sigma_{Taylor}$, where H_{theo} represents the theoretical hardness of the solid solution, $\Delta\sigma_{stress}$, $\Delta\sigma_{HP}$ and $\Delta\sigma_{Taylor}$ represent the contributions from residual stress, GB (Hall–Petch) hardening and strain (Taylor) hardening, respectively. Using value from the former theoretical calculation in reference [9], H_{theo} is 16.6 GPa for TiN and 21.1 GPa for $TiMo_{50}N$, yielding H_{theo} = 19 GPa for $Ti_{31.5}Mo_{9.1}N_{59.4}$ assuming it follows the mixing rule. This is still 14 GPa lower than the actual hardness of 33 GPa, meaning that the other factors should have great influences. The GB hardening $\Delta\sigma_{HP}$ is estimated according to Hall–Petch relation $\Delta\sigma_{HP} = k{\cdot}d^{-1/2}$, where k is constant and d is grain size. Taking a large k = 21.2 GPa·nm$^{1/2}$ for ceramics [34] and d = 56.5 nm, $\Delta\sigma_{HP}$ = 2.8 GPa. The strain hardening is estimated according to the Taylor's law [35]:

$$\Delta\sigma_{Taylor} = \alpha MGb(\sqrt{\rho} - \sqrt{\rho_0}), \quad (1)$$

where α is the hardening factor that range 0.3 – 0.6 for nanocrystals [36] (we used maximum α = 0.6 for ceramics), M is the Taylor factor (about 3.06 [36]), G is the shear modulus, b is the magnitude of Burgers vector $\boldsymbol{B}$. Taking the data from reference [9], G = 171.4 GPa is for TiMoN using mixing rule. As the dislocations visible under $\boldsymbol{g}$ = [111], taking the Burgers vector $\boldsymbol{B}$ = 1/2a[110] (a is the lattice parameter), b is 0.3 nm. For a dislocation density of 2.88 × 10^{11} cm^{-2}, $\Delta\sigma_{Taylor}$ is estimated to be about 5.1 GPa. This indicates that dislocations have significant contribution on the hardness, comparable to GB hardening, and they jointly make a 7.9 GPa increment to hardness. The remaining 6.1 GPa differential could be primarily caused by compressive stress, which implies that compressive stress could pry a hardness increment twice its own value (3 GPa here). Although the quantitative relation between compressive stress and hardness increment remain unclear, this conjecture is supported by previous findings where a superhardness of 41 GPa was achieved under an ultrahigh compressive stress of 6.3 GPa [37].

On the other hand, the improved dislocation activities in the TiMoN coatings also have crucial effect on toughness. It is well established that the intergranular sliding governs the deformation of PVD TMN coatings [38]. Chen et al. revealed that GBs sliding in polycrystalline TiN/AlN superlattice screens dislocation activities, which are responsible for significant strain strenghthening in single-crystalline counterpart [21, 22]. Although it is believed that GB sliding can dissipate deformation energy during deformation [32], our previous study showed that the GB sliding-dominating mode [37] was vulnerable to intergranular cracks [33] when intragranular plasticity is absent. In contrast, our observations identify effective dislocation multiplication in the TiMoN coating. Although the dislocation density is still much lower than fcc nanograined metals [36], such a high density has scarcely been reported for nanocrystalline ceramics. This triggered dislocation-mediated plasticity in TMN coating, offering extra energy dissipation paths, mitigated the stress concentration at GBs, being the key factor for toughness enhancement. This is well showcased by the GB curving (Fig. 3b, e) and the suppressed crack in Fig. 3a that supports the scanning electron microscopic (SEM) observation in Fig. 2a.

Figure 4b depicts the schematic deformation process for the nanocrystalline $TiMo_{27}N$ coating. The pristine structure of the as-deposited coatings comprises nanoscale columnar grains containing numerous deposition-stored dislocations with their GBs pinned by high compressive stress. Therefore, GBs undergo constrained sliding and intergranular cracking is suppressed during the actual deformation. Furthermore, the prestored high-density dislocations provide considerable sources for dislocation to slip, which are then continuously multiplied and absorbed at GBs, generating strain hardening as well as improved plasticity.

In summary, a hard-yet-tough TiMoN coating was prepared via high-ionization arc plating and its deformation behaviors have been thoroughly investigated. Our analysis verifies that dislocation, GBs and compressive stress each have significant contribution on hardness. Furthermore, compressive stress-constrained GB sliding and dislocation slipping collectively predominate the deformation process and result in improved toughness, as testified by GB curving microscopically and surface piling-up

mesoscopically. The highlighted discovery of dislocation-mediated deformation generate new insights on the origins of hardness and toughness of TMN coatings that construct better links between electronic structure and overall mechanical behaviors of ceramic coatings, and imply possibility to tune mechanical properties by manipulating dislocation inside ceramics.

Acknowledgements This work was financially supported by the Distinguished Young Scholars of China (No. 52025014), Natural Science Foundation of Zhejiang Province (No. LQ23E010002) and Innovation 2025 Major Project of Ningbo (Nos. 2022Z011 and 2023Z022).

Declarations

Conflict of interests The authors declare that they have no conflict of interest.

References

[1] Guo T, Chen Y, Cao R, Pang X, He J, Qiao L. Cleavage cracking of ductile-metal substrates induced by brittle coating fracture. Acta Mater. 2018;152:77. https://doi.org/10.1016/j.actamat.2018.04.017.

[2] Shuai J, Zuo X, Wang Z, Guo P, Xu B, Zhou J, Wang A, Ke P. Comparative study on crack resistance of TiAlN monolithic and Ti/TiAlN multilayer coatings. Ceram Int. 2020;46(5):6672. https://doi.org/10.1016/j.ceramint.2019.11.155.

[3] Daniel R, Meindlhumer M, Baumegger W, Zalesak J, Sartory B, Burghammer M, Mitterer C, Keckes J. Grain boundary design of thin films: using tilted brittle interfaces for multiple crack deflection toughening. Acta Mater. 2017;122:130. https://doi.org/10.1016/j.actamat.2016.09.027.

[4] Ren P, Wen M, Zhang K, Du S, Zhang Y, Chen J, Zheng W. Self-assembly of TaC@Ta core–shell-like nanocomposite film via solid-state dewetting: toward superior wear and corrosion resistance. Acta Mater. 2018;160:72. https://doi.org/10.1016/j.actamat.2017.07.034.

[5] Xie Z, Hoffman M, Munroe P, Bendavid A, Martin P. Deformation mechanisms of TiN multilayer coatings alternated by ductile or stiff interlayers. Acta Mater. 2008;56(4):852. https://doi.org/10.1016/j.actamat.2007.10.047.

[6] Buchinger J, Koutna N, Kirnbauer A, Holec D, Mayrhofer P. Heavy-element-alloying for toughness enhancement of hard nitrides on the example Ti-W-N. Acta Mater. 2022;231:117897. https://doi.org/10.1016/j.actamat.2022.117897.

[7] Sangiovanni D, Hultman L, Chirita V, Petrov I, Greene J. Effects of phase stability, lattice ordering, and electron density on plastic deformation in cubic TiWN pseudobinary transition-metal nitride alloys. Acta Mater. 2016;103:823. https://doi.org/10.1016/j.actamat.2015.10.039.

[8] Hu J, Li H, Li J, Yan C, Kong J, Wu Q, Xiong D. Super-hard and tough $Ta_{1-x}W_xC_y$ films deposited by magnetron sputtering. Surf Coat Technol. 2020;400:126207. https://doi.org/10.1016/j.surfcoat.2020.126207.

[9] Sangiovanni D, Hultman L, Chirita V. Supertoughening in B1 transition metal nitride alloys by increased valence electron concentration. Acta Mater. 2011;59(5):2121. https://doi.org/10.1016/j.actamat.2010.12.013.

[10] Li H, Li J, Kong J, Huang J, Wu Q, Xiong D. Hard and tough sub-stoichiometric B1 Ta-Mo-N_x films by regulating N content. J Alloy Compd. 2023;934:168009. https://doi.org/10.1016/j.jallcom.2022.168009.

[11] Kindlund H, Sangiovanni D, Martinez-de-Olcoz L, Lu J, Jensen J, Birch J, Petrov I, Greene J, Chirita V, Hultman L. Toughness enhancement in hard ceramic thin films by alloy design. APL Mater. 2013;1(4):042104. https://doi.org/10.1063/1.4822440.

[12] Mikula M, Truchly M, Sangiovanni D, Plasienka D, Roch T, Gregor M, Durina P, Janik M, Kus P. Experimental and computational studies on toughness enhancement in Ti–Al–Ta–N quaternaries. J Vac Sci Technol A. 2017;35(6):060602. https://doi.org/10.1116/1.4997431.

[13] Mikula M, Plasienka D, Sangiovanni D, Sahul M, Roch T, Truchly M, Gregor M, Caplovic L, Plecenik A, Kus P. Toughness enhancement in highly NbN-alloyed Ti–Al–N hard coatings. Acta Mater. 2016;121:59. https://doi.org/10.1016/j.actamat.2016.08.084.

[14] Sangiovanni D, Chirita V, Hultman L. Toughness enhancement in TiAlN-based quarternary alloys. Thin Solid Films. 2012;520(11):4080. https://doi.org/10.1016/j.tsf.2012.01.030.

[15] Gao Z, Buchinger J, Koutna N, Wojcik T, Hahn R, Mayrhofer P. Ab initio supported development of TiN/MoN superlattice thin films with improved hardness and toughness. Acta Mater. 2022;231:117871. https://doi.org/10.1016/j.actamat.2022.117871.

[16] Liu Y, Li H, Li J, Zhao X, Huang J, Kong J, Wu Q, Shi Y, Zhang G, Xiong D. Effect of W content on mechanical and tribological behaviors of hard $Ta_{1-x}W_xN$ films. Int J Refract Metal Hard Mater. 2023;115:106271. https://doi.org/10.1016/j.ijrmhm.2023.106271.

[17] Zhang R, Gu X, Zhang K, Gao X, Liu C, Chen C. Core electron count as a versatile and accurate new descriptor for sorting mechanical properties of diverse transition metal compounds. Adv Mater. 2023;35(44):2304729. https://doi.org/10.1002/adma.202304729.

[18] Hu J, Shi Y, Sauvage X, Sha G, Lu K. Grain boundary stability governs hardening and softening in extremely fine nanograined metals. Science. 2017;355(6331):1292. https://doi.org/10.1126/science.aal5166.

[19] Schiøtz J, Jacobsen K. A maximum in the strength of nanocrystalline copper. Science. 2003;301(5638):1357. https://doi.org/10.1126/science.1086636.

[20] Carvalho N, De Hosson J. Deformation mechanisms in TiN/(Ti, Al)N multilayers under depth-sensing indentation. Acta Mater. 2006;54(7):1857. https://doi.org/10.1016/j.actamat.2005.12.010.

[21] Chen Z, Zheng Y, Huang Y, Gao Z, Sheng H, Bartosik M, Mayrhofer P, Zhang Z. Atomic-scale understanding of the structural evolution in TiN/AlN superlattice during nanoindentation—Part 2: strengthening. Acta Mater. 2022;234:118009. https://doi.org/10.1016/j.actamat.2022.118009.

[22] Chen Z, Zheng Y, Huang Y, Gao Z, Sheng H, Bartosik M, Mayrhofer P, Zhang Z. Atomic-scale understanding of the structural evolution of TiN/AlN superlattice during nanoindentation— Part 1: deformation. Acta Mater. 2022;234:118008. https://doi.org/10.1016/j.actamat.2022.118008.

[23] Pao C, Foiles S, Webb E, Srolovitz D, Floro J. Thin film compressive stresses due to adatom insertion into grain boundaries. Phys Rev Lett. 2007;99(3):036102. https://doi.org/10.1103/PhysRevLett.99.036102.

[24] Stoney G, Parsons C. The tension of metallic films deposited by electrolysis. Proceedings of the Royal Society of London. Series A Containing Papers of a Mathematical and Physical Character. 1909;82(553):172. https://doi.org/10.1098/rspa.1909.0021.

[25] Zhao J, Wang X, Chen Z, Yang S, Shi T, Liu X. Overall energy model for preferred growth of TiN films during filtered arc deposition. J Phys D Appl Phys. 1997;30(1):5. https://doi.org/10.1088/0022-3727/30/1/002.

[26] Zhou S, Zhao W, Qiu Z, Lin S, Zheng Z, Zeng D. Improved load-bearing capacity of Mo-doped Ti–N coatings: effects of Mo

alloying and GB plasticity. Surf Coat Technol. 2021;424:127630. https://doi.org/10.1016/j.surfcoat.2021.127630.

[27] Zhang Z, Ghasemi A, Koutná N, Xu Z, Grünstäudl T, Song K, Holec D, He Y, Mayrhofer P, Bartosik M. Correlating point defects with mechanical properties in nanocrystalline TiN thin films. Mater Des. 2021;207:109844. https://doi.org/10.1016/j.matdes.2021.109844.

[28] Chen J, Lu L, Lu K. Hardness and strain rate sensitivity of nanocrystalline Cu. Scripta Mater. 2006;54(11):1913. https://doi.org/10.1016/j.scriptamat.2006.02.022.

[29] Lüthy H, White R, Sherby O. Grain boundary sliding and deformation mechanism maps. Mater Sci Eng. 1979;39(2):211. https://doi.org/10.1016/0025-5416(79)90060-0.

[30] Wei Y, Bower A, Gao H. Enhanced strain-rate sensitivity in fcc nanocrystals due to grain-boundary diffusion and sliding. Acta Mater. 2008;56(8):1741. https://doi.org/10.1016/j.actamat.2007.12.028.

[31] Sahu B, Dutta A, Mitra R. Mechanism of negative strain rate sensitivity in metallic glass film. J Alloy Compd. 2019;784:488. https://doi.org/10.1016/j.jallcom.2019.01.024.

[32] Li Z, Munroe P, Jiang Z, Zhao X, Xu J, Zhou Z, Jiang J, Fang F, Xie Z. Designing superhard, self-toughening CrAlN coatings through grain boundary engineering. Acta Mater. 2012;60(16):5735. https://doi.org/10.1016/j.actamat.2012.06.049.

[33] Zhou S, Qiu Z, Zeng D. Deformation mechanisms and crack routes of CrAlN coatings. Mater Charact. 2020;167:110491. https://doi.org/10.1016/j.matchar.2020.110491.

[34] Ryou H, Drazin J, Wahl K, Qadri S, Gorzkowski E, Feigelson B, Wollmershauser J. Below the Hall-Petch limit in nanocrystalline ceramics. ACS Nano. 2018;12(4):3083. https://doi.org/10.1021/acsnano.7b07380.

[35] Wang Y, Ott R, Hamza A, Besser M, Almer J, Kramer M. Achieving large uniform tensile ductility in nanocrystalline metals. Phys Rev Lett. 2010;105(21):215502. https://doi.org/10.1103/PhysRevLett.105.215502.

[36] Li H, Zong H, Li S, Jin S, Chen Y, Cabral M, Chen B, Huang Q, Chen Y, Ren Y, Yu K, Han S, Ding X, Sha G, Lian J, Liao X, Ma E, Sun J. Uniting tensile ductility with ultrahigh strength via composition undulation. Nature. 2022;604(7905):273. https://doi.org/10.1038/s41586-022-04459-w.

[37] Zhou S, Kuang T, Qiu Z, Zeng D, Zhou K. Microstructural origins of high hardness and toughness in cathodic arc evaporated Cr-Al-N coatings. Appl Surf Sci. 2019;493:1067. https://doi.org/10.1016/j.apsusc.2019.07.051.

[38] Verma N, Cadambi S, Jayaram V, Biswas S. Micromechanisms of damage nucleation during contact deformation of columnar multilayer nitride coatings. Acta Mater. 2012;60(6):3063. https://doi.org/10.1016/j.actamat.2012.02.011.